

# Multistep Continuous Heterogeneous Synthesis of C.I. Reactive Red 195 and Safety Evaluation of the Continuous Diazotization Process

Lei Li, Xinyu Ye, Huaixi Liu, Rongwen Lu, Bingtao Tang, and Shufen Zhang\*



Cite This: *Org. Process Res. Dev.* 2025, 29, 1168–1178



Read Online

ACCESS |

Metrics & More

Article Recommendations

Supporting Information

**ABSTRACT:** Integrating the diazotization and coupling reactions in solid–liquid heterogeneous systems to achieve large-scale, multistep continuous flow synthesis of water-soluble azo dyes remains a significant challenge. During the diazotization process of water-soluble azo dyes, considerable diazonium salt may precipitate, posing potential safety risks. In this study, we established a continuous dynamic tubular reaction system to achieve the multistep continuous heterogeneous synthesis of C.I. Reactive Red 195, a representative water-soluble azo dye. The optimal conditions for continuous diazotization and coupling reactions were determined, achieving a high throughput of 120 L/h and a yield of up to 736 kg/day. The purity of the synthesized dye increased by 20% compared to the commercial C.I. Reactive Red 195, with the K/S value rising from 19.07 to 22.16, indicating enhanced dyeing performance. Density functional theory (DFT) calculations and ab initio molecular dynamics (AIMD) simulations show that 2-naphthylamine-1,5-disulfonic acid diazonium salt (NADA-DS) spontaneously aggregates into stable clusters due to dispersion forces, which leads to precipitation. Furthermore, the thermal stability, impact sensitivity, explosive propagation, and decomposition activation energy of NADA-DS were investigated. The severity and possibility of thermal runaway during the continuous diazotization process are classified as level 1. The risk matrix indicates that the continuous diazotization process risk is acceptable, with the Stoessel criticality diagram categorizing the hazard level as grade 1, signifying a low level of risk. This study promotes safer, more efficient, and sustainable production of water-soluble azo dyes.

**KEYWORDS:** C.I. Reactive Red 195, multistep continuous synthesis, heterogeneous, process safety

## 1. INTRODUCTION

Azo dyes are widely utilized in various industries such as textiles,<sup>1</sup> coatings,<sup>2</sup> food,<sup>3</sup> leather,<sup>4</sup> inks,<sup>5</sup> cosmetics,<sup>6</sup> and biomedical research<sup>7</sup> due to their vibrant colors, broad color range, and easy access to raw materials. Typically, azo dyes containing both monochlorotriazine and  $\beta$ -hydroxyethyl sulfone sulfate groups, which can react with the hydroxyl groups of cotton fibers to form chemical bonds, are selected for dyeing cotton to achieve excellent washing fastness.<sup>8</sup> C.I. Reactive Red 195 serves as a typical example of this dye type, with its synthetic route depicted in Figure 1. Initially, 2-naphthylamine-1,5-disulfonic acid (NADA) undergoes diazotization to produce 2-naphthylamine-1,5-disulfonic acid diazonium salt (NADA-DS) (Figure 1a), which then couples with 4-[[4-chloro-6-[[4-[[2-(sulfooxy)ethyl]sulfonyl]phenyl]-amino]-1,3,5-triazin-2-yl]amino]-5-hydroxy-2,7-naphthalenedisulfonic acid (CTN) to synthesize C.I. Reactive Red 195 (Figure 1b). At the industrial scale, azo dyes are typically produced in batch reactors with capacities of several tens of cubic meters,<sup>9</sup> which results in inefficiencies in mass and heat transfer and poses potential safety hazards due to the presence of diazonium salts.<sup>10–12</sup> In the case of C.I. Reactive Red 195, the significant precipitation of diazonium salt during diazotization further complicates the manufacturing process, highlighting the need for safer and more efficient large-scale production methods.

During the production of C.I. Reactive Red 195, the precipitation of diazonium salts may pose potential safety

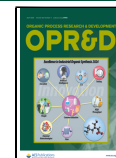
hazards. For instance, Ullrich reported an explosion caused by the mechanical cleaning of a valve contaminated with dried, precipitated diazonium salts.<sup>13</sup> Sheng et al. highlighted several industrial accidents, including explosions, fatalities, and property damage resulting from unintended precipitation.<sup>14</sup> Consequently, the safety of diazotization processes and the thermal stability of diazonium salts have garnered significant attention in recent years. Nielsen et al. conducted a safety evaluation of a new diazotization process for 2-chloro-5-trifluoromethylaniline, enabling the safe scaling-up of the Sandmeyer reaction.<sup>15</sup> Zhang et al. assessed the thermal hazard of the glycine methyl ester diazotization reaction and its product, methyl diazoacetate, through calorimetric analysis, concluding it posed a low risk.<sup>16</sup> Cheng et al. analyzed the thermal risk of 2-methoxy-4-nitroaniline diazotization using calorimetric analysis and kinetic parameter calculations, finding it to be at risk level 2.<sup>17</sup> Other studies have investigated the thermal stability of various diazonium salts, such as aniline diazonium salts,<sup>18</sup> arenediazonium tetrafluoroborate salts,<sup>19,20</sup> and arenediazonium triflates.<sup>21</sup> However, research on the thermal stability of NADA-DS and the safety of its synthesis

Received: February 18, 2025

Revised: March 11, 2025

Accepted: March 18, 2025

Published: March 27, 2025



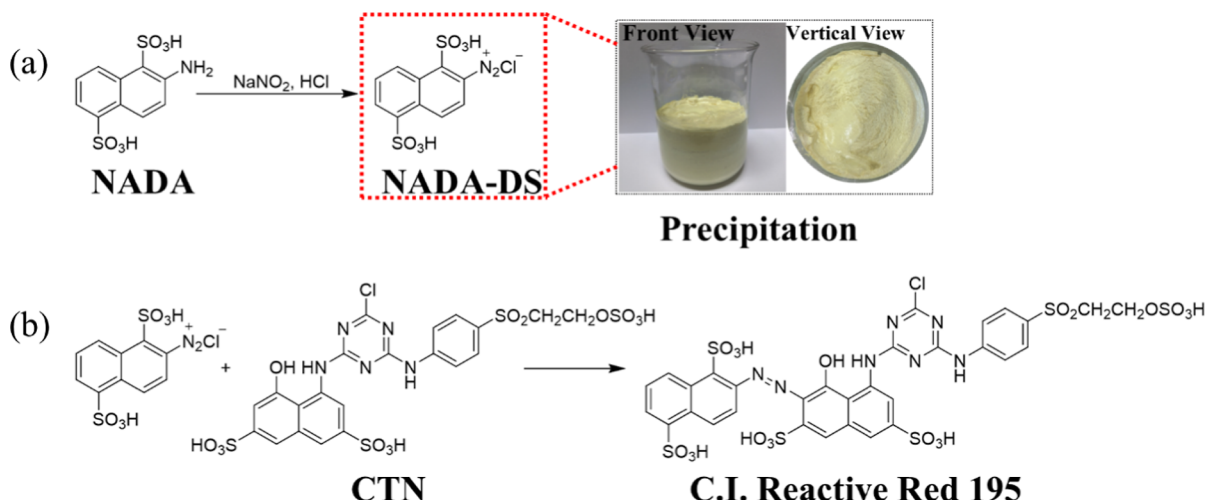


**Figure 1.** Synthesis route of C.I. Reactive Red 195: (a) diazotization, (b) coupling.

process remains absent, which is essential for improving the C.I. Reactive Red 195 production and ensuring safety.

Unlike traditional batch operations, continuous flow technology offers several advantages, including high mass and heat transfer efficiency, stable product quality, and a compact footprint.<sup>22–24</sup> Recently, researchers have conducted continuous coupling reactions in a microreactor, using prepared diazonium salts and coupling components, to synthesize water-insoluble azo dyes or pigments, such as Pigment Yellow 12,<sup>25,26</sup> Pigment Yellow 14,<sup>27</sup> C.I. Reactive Red 195,<sup>28</sup> and Pigment Red 146.<sup>29</sup> The above studies typically use dilute feed conditions or organic solvents to prevent reactor clogging. To avoid clogging in a heterogeneous solid–liquid system, Sharma et al. utilized a single-screw reactor to produce Sudan I with a throughput of 2.4 L/h.<sup>30</sup> Shukla et al. employed a bubble column reactor to continuously synthesize Solvent Yellow 16 at a 5 wt % slurry concentration, producing approximately 1.92 kg/day.<sup>12</sup> However, most research focuses on continuous coupling to synthesize water-insoluble azo dyes, few studies have investigated continuous diazotization and coupling in solid–liquid heterogeneous systems for producing water-soluble azo dyes.

In this study, we designed a continuous dynamic tubular reaction system for the multistep continuous heterogeneous synthesis of C.I. Reactive Red 195. The reaction conditions of continuous diazotization and coupling reactions were investigated. The resulting dye was compared with commercial C.I. Reactive Red 195 in terms of purity, color depth, and color fastness. We also examined the influence of intermolecular interactions on NADA-DS precipitation, analyzed its thermal stability, impact sensitivity, and explosive propagation characteristics, and calculated its decomposition activation energy. Moreover, the safety of the continuous diazotization process was evaluated. This research provides new insights into the safer, more efficient, and sustainable production of water-soluble azo dyes.

## 2. EXPERIMENTAL SECTION

**2.1. Materials.** 1-Naphthol (analytical grade, ≥99 wt %) and sulfanilic acid (analytical grade, 99 wt %) were purchased from Shanghai Aladdin Biochemical Technology Co., Ltd. 4-(Ethylsulfurfonyl)aniline (technical grade, 96 wt %), 2-amino-1,5-naphthalenedisulfonic acid (technical grade, 79.42

wt %), cyanuric chloride (technical grade, ≥99 wt %), and H acid (technical grade, 85.56 wt %) were obtained from Jiangsu Demeike Chemical Co., Ltd. Sodium nitrite (analytical grade, ≥99 wt %) and sulfamic acid (analytical grade, ≥99 wt %) were purchased from Tianjin Damao Chemical Reagent Co., Ltd. Hydrochloric acid (analytical grade, 36 wt %) was sourced from Fuyu Chemical Reagent Factory. Sodium carbonate (analytical grade, ≥99 wt %), and sodium bicarbonate (analytical grade, ≥99 wt %) were procured from Tianli Chemical Reagent Co., Ltd. C.I. Reactive Red 195 (commercially available) was supplied by Jiangsu Jinji Industrial Co., Ltd. All other chemicals used in this study were of synthetic-grade purity.

**2.2. Instruments.** The thermal analysis equipment includes the DSC (DSC2500, TA Instruments), TGA (Q500, TA Instruments), and a reaction calorimeter (EasyMax 402 HFCal, Mettler Toledo). The continuous reaction system incorporates a dynamic tubular reactor, PLC control cabinet, high–low temperature circulating chiller, and constant flow pumps, all sourced from Shandong Weijing Chemical Technology Co., Ltd. The spray dryer is provided by Beijing Holmes Biotechnology Co., Ltd. Sample analysis is conducted using HPLC (1260, Agilent), MS (6130, Agilent), and FTIR (6700, Thermo Fisher). Dyeing equipment is the ECO DYER from Xiamen Rapid Precision Machinery Co., Ltd. Color evaluation equipment comprises the rubbing fastness tester, light fastness tester, both from Wenzhou Darong Textile Instrument Co., Ltd., and the UltraScan Pro colorimeter from Hunter Associates Laboratory, Inc.

**2.3. Characterization of Mixing.** The Bourne reaction,<sup>31</sup> also known as the Diazo coupling reaction, has been widely used to characterize the mixing efficiency of various reactors.<sup>32–34</sup> The specific reaction formula and details can be found in the Supporting Information. In this study, the reaction system was employed to assess the mixing efficiency in a dynamic tubular reactor, with the segregation index ( $X_S$ ) determined based on product concentration measurements.

**2.4. Preparation of Feed Solution.** The raw material solutions included NADA (0.5 mol/L), sodium nitrite (5.3 mol/L), hydrochloric acid (6 mol/L), sulfamic acid (1.5 mol/L), and CTN (0.5 mol/L), all in aqueous solutions. Taking the preparation process of the NADA aqueous solution as an example (due to the similarity in the preparation processes for

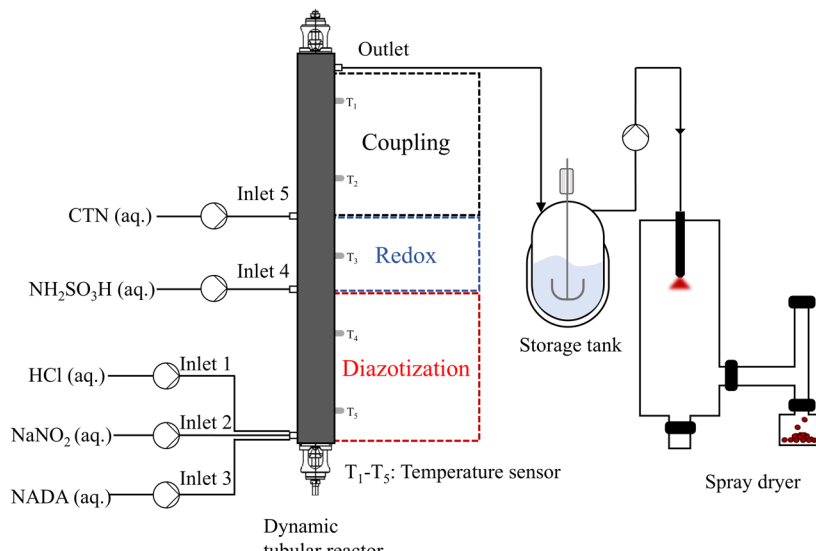


**Figure 2.** Process for the continuous flow synthesis of C.I. Reactive Red 195.

all raw material solutions): 12.5 mol of NADA was added to a 50 L stirring kettle, followed by water to the 25 L mark, and the mixture was stirred until dissolved. Finally, impurities were removed by filtration, and the concentration was determined via diazotization titration.

**2.5. Experimental Procedure for Continuous Process.** Details of the continuous flow experimental setup are provided in the *Supporting Information* section. The continuous flow synthesis process of C.I. Reactive Red 195 is illustrated in Figure 2. Before the reaction, the mechanical stirrer is activated first to ensure proper mixing of the reactants. The reaction temperature is then controlled by a high–low temperature circulating chiller to maintain the desired temperature throughout the process. The flow rates and start times of the pumps are controlled by a PLC control panel. Based on the preset start times, the pumps delivering NADA, hydrochloric acid, and sodium nitrite solutions are activated simultaneously to transport the three raw materials to the bottom of the tubular reactor. The raw materials flow upward through the reactor and undergo diazotization in the corresponding zone, producing diazonium salts. When the reactant mixture reaches “Inlet 4”, the pump delivering a sulfamic acid solution is activated, directing it to the oxidation–reduction zone of the reactor, where excess nitrite is eliminated. Upon reaching “Inlet 5”, the pump delivering the CTN solution is activated, transporting the solution to the coupling zone, where it mixes with diazonium salts and undergoes a coupling reaction to form the target dye. The product is then discharged from the top of the reactor into the storage tank for a 5 min delayed reaction to ensure complete conversion. Finally, the liquid dye is dried into powder by the spray dryer for subsequent processing and analysis. The dye purity is analyzed by HPLC at a wavelength of 254 nm using the peak area normalization method.

**2.6. Dyeing Process.** Cotton fibers were dyed using both the dyes synthesized in this study and commercial C.I. Reactive Red 195. The procedure was as follows: First, 2 g of cotton fibers and 0.04 g of C.I. Reactive Red 195 were added to a 40 mL aqueous solution. Subsequently, the samples were placed in an ECO DYER and dyed at room temperature for 30 min, with 2 g of sodium sulfate added every 15 min. The

temperature was gradually increased to 60 °C at a rate of 2 °C/min, and 0.4 g of sodium carbonate was added for color fixation for 40 min. After dyeing, the fabric samples were removed and washed with water to remove residual dye and then placed in 100 mL of an aqueous solution containing 2% White Cat Laundry Detergent. The solution was heated to 90 °C, and washed for 10 min. Finally, the fabric samples were taken out, rinsed thoroughly with water, and dried for subsequent analysis.

**2.7. Color Fastness and Color Depth Assessment.** The washing fastness was tested according to ISO 105-C10:2006. The rubbing fastness was tested according to ISO 105-X12:2016. The light fastness was tested according to ISO 105-B02:2014. K/S values were calculated using an Ultrascan Pro colorimeter with D65 illumination and a 10° standard observer.

**2.8. Theoretical Calculation.** Geometry optimization and frequency analysis of the NADA-DS dimer were performed using Gaussian 16 at the B3LYP-D3(BJ)/6–31+G(d,p) level with the PCM solvent model.<sup>35–38</sup> Subsequently, wave function analysis was performed using Multiwfn 3.8 (dev),<sup>39</sup> based on the aforementioned computational results. Non-covalent interaction (NCI) isosurface diagrams were generated using VMD software<sup>40</sup> based on Multiwfn exported files. Energy decomposition analysis (EDA) was conducted using the Psi4 program<sup>41</sup> at the sSAPT0/jun-cc-pVDZ level of theory. AIMD simulations were conducted using the xtb software at the GFN1-xTB level with the ALPB implicit solvation model.<sup>42</sup> The simulations were conducted for 100 ps in the NVT ensemble at  $T = 298.15$  K with a time step of 2 fs and temperature controlled by the Berendsen thermostat.

**2.9. DSC Measurement of NADA-DS.** DSC was used to preliminarily assess the thermal hazards of the reactant species, providing a basis for subsequent research. The heat of reaction for the decomposition of approximately 2 mg of NADA-DS was measured in a closed crucible at a ramp rate of 2 °C/min from 25 to 250 °C with an N<sub>2</sub> purge. Each experiment was repeated at least three times.

**2.10. TGA Measurement of NADA-DS.** TGA was used to assess the thermal stability of NADA-DS. The test samples (1.2–1.4 mg) were heated from 25 to 250 °C at heating rates

of 8, 10, 12, and 15 °C/min. Each experiment was repeated at least three times for each condition.

### 2.11. Calorimetric Testing of Diazotization Reaction.

The safety of the NADA diazotization process was evaluated using a reaction calorimeter. The reactant temperature was controlled isothermally using the EasyMax 402 HFCal system. Initially, 29.40 g (0.077 mol) of NADA and 135 g of deionized water were added to the reactor. The temperature was lowered to 5 °C with the stirring speed set to 300 rpm. Subsequently, 15.25 g of sodium nitrite solution (30 wt %) was rapidly added, and the reaction was allowed to proceed for 30 min. After the reaction was completed, the temperature was gradually raised to room temperature. During the reaction, parameters including reactor temperature ( $T_r$ ), jacket temperature ( $T_j$ ), stirring rate ( $R$ ), and heat release rate ( $q_r$ ) were recorded. The heat release of the diazotization ( $\Delta H_r$ ) was calculated by integrating  $q_r$ , with the baseline determined by the line connecting the initial and final points of the reaction curve.

## 3. RESULT AND DISCUSSION

**3.1. Characterization of Mixing.** The mixing performance of the reactor is critical to the reaction outcome,<sup>43</sup> as it directly impacts both the efficiency and selectivity. To evaluate the mixing efficiency, a competitive consecutive reaction system (Bourne reaction) was employed. As shown in Figure 3, with an increase in rotation speed, the segregation index

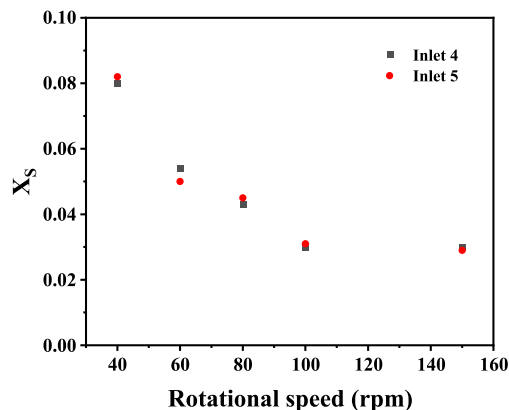


Figure 3. Relationship between rotational speed and segregation index.

( $X_s$ ) decreases, indicating better mixing performance. The minimum  $X_s$  value is approximately 0.03, close to zero, indicating that the reactor provides nearly ideal mixing conditions, ensuring uniform distribution of reactants. Whether 1-naphthol is fed through Inlet 4 or Inlet 5, the mixing efficiency remains stable. This demonstrates that the material can be efficiently mixed regardless of the inlet used. Considering both energy consumption and reaction efficiency, a rotation speed of 100 rpm was selected as the optimal condition for the subsequent continuous synthesis of C.I. Reactive Red 195.

### 3.2. Optimization of Continuous Flow Reaction Conditions.

In the multistep continuous flow synthesis of C.I. Reactive Red 195, the diazotization and coupling reactions are critical steps.<sup>44</sup> Transitioning from batch production to continuous-flow processes requires comprehensive optimization of key reaction parameters, which focus primarily on the

molar ratio, temperature, pH, and total flow rate to ensure reaction efficiency and stable continuous-flow operation.

### 3.2.1. Optimization of Continuous Diazotization Reaction Conditions.

Given the inherent acidity of NADA, it is essential to determine the optimal amount of hydrochloric acid for diazotization. As illustrated in Figure 4a, the yield of diazonium salts remains stable as the molar ratio (HCl/NADA) increases from 0 to 2.0, indicating that the acidity of the NADA raw materials is sufficient for the diazotization reaction, and additional acid is unnecessary. To investigate the effect of sodium nitrite dosage on the diazotization reaction, the molar ratio ( $\text{NaNO}_2/\text{NADA}$ ) was varied from 1 to 1.1. The yield of diazonium salts initially increased, peaking at a ratio of 1.05, then decreased (Figure 4b). This is because excess sodium nitrite may prevent the reaction between NADA and NADA-DS, while also promoting the progression of the diazotization reaction. However, too much sodium nitrite produces extra nitrous acid, leading to diazonium salt decomposition.<sup>45</sup> Therefore, the optimal  $\text{NaNO}_2/\text{NADA}$  molar ratio is 1.05:1.

### 3.2.2. Optimization of Continuous Coupling Reaction Conditions.

To determine the optimal conditions for the coupling reaction, the effects of temperature, pH of CTN (coupling component) solution, and total flow rate on dye purity were investigated. The reaction temperature significantly affects both the reaction rate and selectivity of the reactants. As shown in Figure 5a, increasing the reaction temperature from 5 to 20 °C accelerated the reaction and enhanced system flowability, resulting in higher dye purity within the same residence time. However, a further temperature rise significantly increases the hydrolysis of the dye and diazonium salt, causing a decrease in dye purity. Increasing the pH of the CTN solution from 7 to 10 also improved dye purity to approximately 90%, as the hydroxyl group of CTN was converted into oxyanion under alkaline conditions, thereby increasing the reactivity of the coupling site and the coupling reaction rate. However, a further increase in the pH led to reduced dye purity due to dye hydrolysis (Figure 5b). Finally, varying the total flow rate from 1000 to 2000 mL/min had little effect on dye purity, indicating effective mass and heat transfer in the dynamic tubular reactor (Figure 5c). As the total flow rate increased, the reaction times for each step decreased: the diazotization reaction time was reduced from 142 to 71 s, the oxidation–reduction step from 68 to 34 s, the coupling reaction from 77 to 39 s, and the overall residence time from 287 to 144 s (Figure 5d). In conclusion, the optimal conditions are as follows:  $T_p = 20$  °C,  $pH = 10$ , and  $Q = 2000$  mL/min.

**3.2.3. Comparison of Dye Performance by Different Synthesis Methods.** After optimization, the productivity of C.I. Reactive Red 195 reached 736 kg/day, with a throughput of 120 L/h. Mass spectrometry analysis revealed a molecular ion peak at 511.5 ( $[\text{M} - 2\text{H}]^{2-}/2$ ), consistent with the molecular weight of C.I. Reactive Red 195 (Figure 6a). The infrared spectrum showed characteristic peaks consistent with C.I. Reactive Red 195, further confirming the compound structure (Figure 6b). In addition, liquid chromatography chromatograms for both commercial and continuously synthesized C.I. Reactive Red 195 displayed identical retention times for the main products (Figure 6c). Notably, the continuously synthesized C.I. Reactive Red 195 achieved approximately 25% higher purity than the commercial dye (Figure 6d).

The two dyes were used to color cotton fabrics, and their color depth and color fastness were compared (Table 1). The

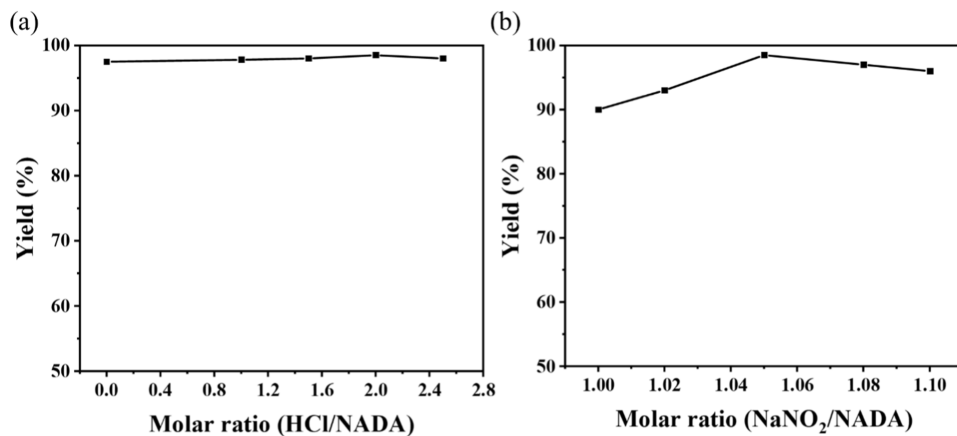


**Figure 4.** Optimization of continuous diazotization reaction conditions. (a) Effect of the molar ratio of hydrochloric acid to NADA on diazotization yield. Conditions:  $n(\text{NaNO}_2)/n(\text{NADA}) = 1.05$ ,  $Q = 1000 \text{ mL/min}$ ,  $T_p = 10^\circ\text{C}$ . (b) Effect of the molar ratio of sodium nitrite to NADA on diazotization yield. Conditions:  $n(\text{HCl})/n(\text{NADA}) = 0$ ,  $Q = 1000 \text{ mL/min}$ ,  $T_p = 10^\circ\text{C}$ .

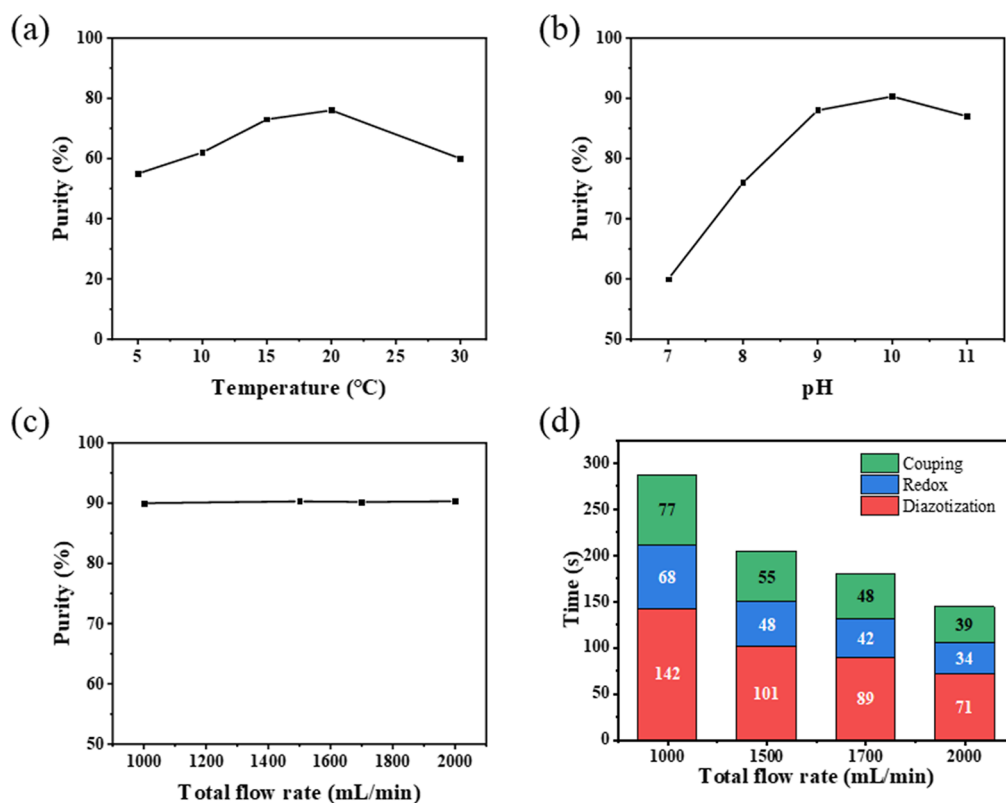


**Figure 5.** Optimization of continuous coupling reaction conditions. (a) Effect of temperature on dye purity. Conditions:  $n(\text{NaNO}_2)/n(\text{NADA}) = 1.05$ ,  $n(\text{HCl})/n(\text{NADA}) = 0$ ,  $n(\text{NH}_2\text{SO}_3\text{H})/n(\text{NADA}) = 0.05$ ,  $\text{pH} = 8$ ,  $Q = 1000 \text{ mL/min}$ . (b) Effect of CTN solution pH on dye purity. Conditions:  $n(\text{NaNO}_2)/n(\text{NADA}) = 1.05$ ,  $n(\text{HCl})/n(\text{NADA}) = 0$ ,  $n(\text{NH}_2\text{SO}_3\text{H})/n(\text{NADA}) = 0.05$ ,  $T_p = 20^\circ\text{C}$ ,  $Q = 1000 \text{ mL/min}$ . (c) Effect of total flow rate on dye purity. Conditions:  $n(\text{NaNO}_2)/n(\text{NADA}) = 1.05$ ,  $n(\text{HCl})/n(\text{NADA}) = 0$ ,  $n(\text{NH}_2\text{SO}_3\text{H})/n(\text{NADA}) = 0.05$ ,  $T_p = 20^\circ\text{C}$ ,  $\text{pH} = 10$ . (d) The relationship between the reaction time and the total flow rate for each reaction step within the tubular reactor.

*K/S* value in the table is a critical indicator for evaluating dyeing performance by quantifying the color depth on dyed textile surfaces. The continuously produced dye showed superior performance, with a *K/S* value of 22.16, significantly higher than the 19.07 of the commercial dye. Rubbing, washing, and light fastness, influenced by both dye-fiber binding method and dye molecular structure, showed comparable performance for both dyes.

### 3.3. Precipitation Mechanism of NADA-DS

Understanding the precipitation behavior of diazonium salts in an

aqueous solution is important for guiding the safe production of C.I. Reactive Red 195. NADA-DS precipitation is influenced by intermolecular interactions, with dimers—the simplest form of molecular aggregation—commonly used as models to study these interactions due to the complexity of modeling multimolecular aggregation.<sup>46,47</sup> Therefore, the NADA-DS dimer is employed as a model to investigate NADA-DS molecular interactions. In this study, the NADA-DS dimer model was optimized through DFT calculations (Figure 7a), with noncovalent interaction analysis (NCI) revealing

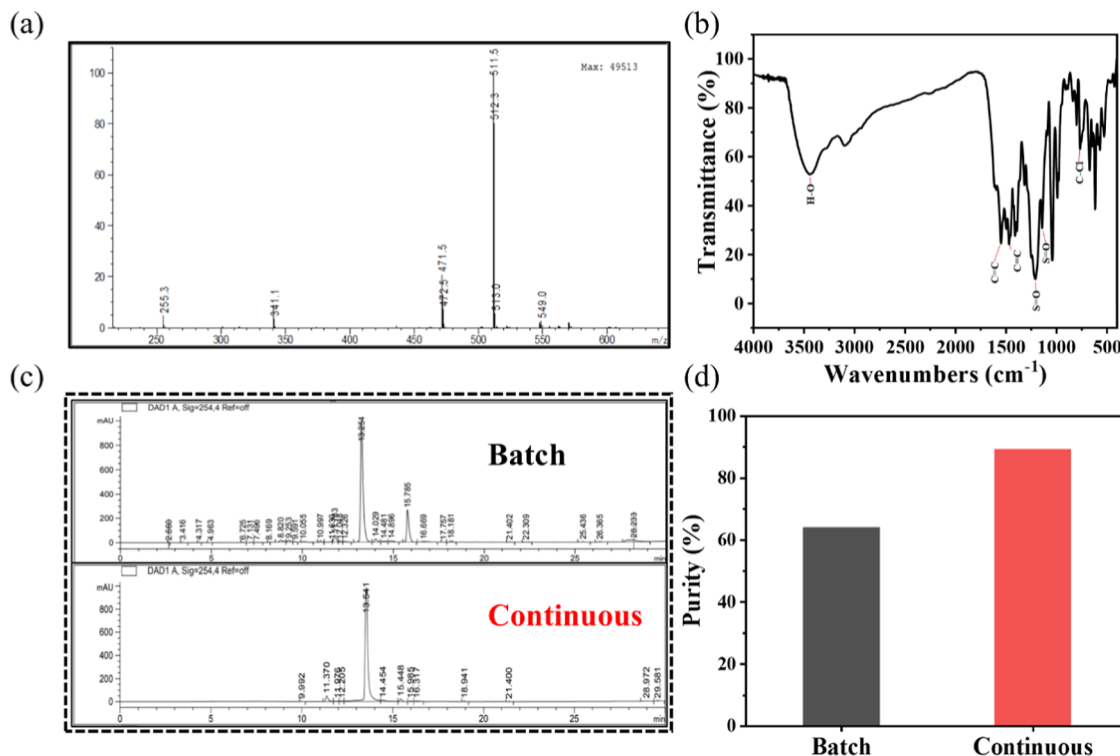


**Figure 6.** Characterization of C.I. Reactive Red 195 synthesized by different methods. (a) Mass spectrum of C.I. Reactive Red 195. (b) Infrared spectrum of C.I. Reactive Red 195. (c) Liquid chromatography chromatograms of C.I. Reactive Red 195 synthesized by different methods. (d) Comparison of dye purity between batch and continuous synthesis methods.

**Table 1. Comparison of Color Depth and Color Fastness**

synthetic process	K/S	rubbing fastness		washing fastness		light fastness	
		dry	wet	change	cotton	wool	
batch	19.07	4–5	4–5	4–5	4–5	4–5	4–5
continuous	22.16	4–5	4–5	4–5	4–5	4–5	4–5

significant  $\pi-\pi$  stacking between NADA-DS molecules (Figure 7b). To further investigate the nature of weak interactions between NADA-DS molecules, symmetry-adapted perturbation theory (SAPT) was employed to conduct energy decomposition analysis (EDA) of their intermolecular interactions, breaking down intermolecular interaction energy ( $\Delta E_{\text{int}}$ ) into multiple physically meaningful energy components, as shown in eq 1. These components include electrostatic ( $\Delta E_{\text{elst}}$ ), exchange ( $\Delta E_{\text{exch}}$ ), dispersion ( $\Delta E_{\text{disp}}$ ), and induction ( $\Delta E_{\text{ind}}$ ). EDA calculations concluded that  $\Delta E_{\text{int}}$  of the NADA-DS dimer is  $-6.73$  kcal/mol, with  $\Delta E_{\text{elst}} = 2.66$  kcal/mol,  $\Delta E_{\text{exch}} = 33.27$  kcal/mol,  $\Delta E_{\text{disp}} = -30.27$  kcal/mol, and  $\Delta E_{\text{ind}} = -12.39$  kcal/mol (Figure 7c). Ab initio molecular dynamics (AIMD) simulations were conducted to assess the stability and atomic thermal motion of the NADA-DS dimer more accurately. Results show that the dimer is highly stable and resistant to dissociation (Figure 7d–f). In summary, following the conversion of NADA to NADA-DS, electrostatic repulsion decreases while dispersion forces dominate, causing NADA-DS molecules to aggregate into stable clusters and precipitate in water spontaneously.

$$\Delta E_{\text{int}} = \Delta E_{\text{elst}} + \Delta E_{\text{exch}} + \Delta E_{\text{disp}} + \Delta E_{\text{ind}} \quad (1)$$

### 3.4. Thermal Stability Risk Assessment of NADA-DS.

#### 3.4.1. Thermal Stability Test of NADA-DS by DSC and TGA.

Due to the general thermal instability of diazonium salts, DSC

was used to analyze the thermal stability of NADA-DS. Figure 8a displays the DSC curve of NADA-DS, revealing with an initial decomposition temperature ( $T_{\text{init}}$ ) of  $71.89$  °C, an extrapolated onset temperature ( $T_{\text{onset}}$ ) of  $86.39$  °C, and a peak temperature ( $T_{\text{peak}}$ ) of  $93.46$  °C. Integration of the peak area yields a decomposition enthalpy ( $\Delta H_d$ ) of  $227.95$  J/g, which is below  $400$  J/g, indicating a decomposition heat risk level of 1 and a potential explosive hazard. TGA data show an approximately 15% thermal weight loss of NADA-DS (Figure 8b). Moreover, TGA measurements at different heating rates provide crucial data for calculating the activation energy of thermal decomposition, as discussed below. The DTG curve is smooth with a single sharp peak corresponding to the weight loss (Figure 8c), indicating that NADA-DS decomposes in a one-step reaction.

**3.4.2. Impact Sensitivity and Explosive Propagation of NADA-DS.** Due to potential collisions between the advancing mechanical stirring shaft and diazonium salts in the dynamic tube reactor, it is necessary to evaluate the impact sensitivity and explosion propagation characteristics of NADA-DS. Yoshida and Pfizer's mathematical correlations (eqs 2–5) are widely used to predict the impact sensitivity (IS) and/or explosive propagation (EP) of organic compounds.<sup>48,49</sup> Both correlations rely on DSC data, including  $T_{\text{init}}$ ,  $T_{\text{onset}}$ , and  $\Delta H_d$ . For the two types of correlations, positive values indicate that a compound is sensitive to impact and/or an explosive

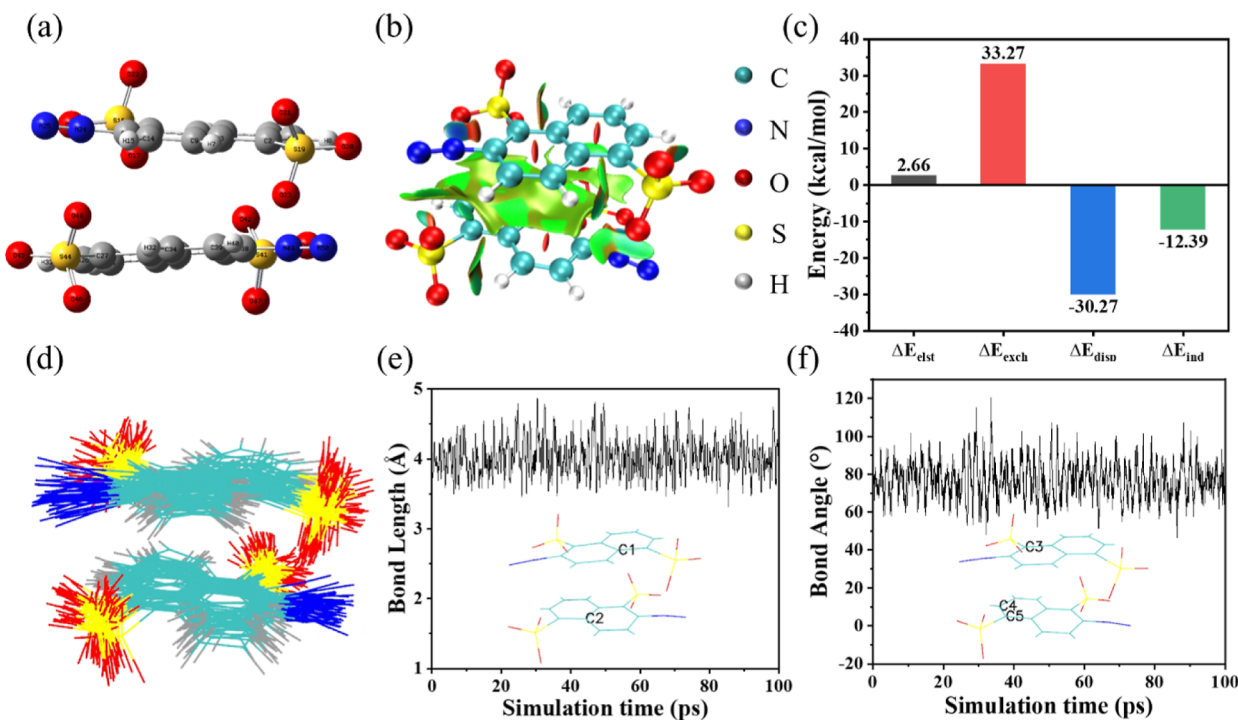


**Figure 7.** Effect of intermolecular interactions on NADA-DS molecule precipitation behavior. (a) Optimal structure of the NADA-DS dimer. (b) Noncovalent interaction analysis of NADA-DS dimer. (c) Energy decomposition analysis of NADA-DS dimer. (d) Overlay of the structural variations of the NADA-DS dimer during the 100 ps AIMD simulation at 298.15 K. (e) Evolution of the C1–C2 bond length in the NADA-DS dimer at 298.15 K. (f) Evolution of the C3–C4–C5 bond angle in the NADA-DS dimer at 298.15 K.

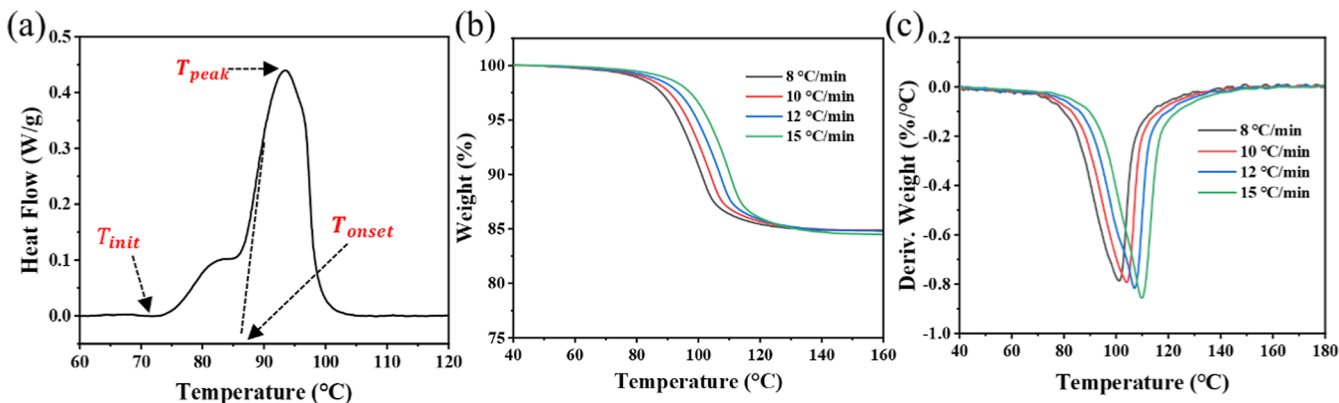


**Figure 8.** Thermal stability of NADA-DS. (a) DSC curve of NADA-DS thermal decomposition. (b) TGA curves of the NADA-DS thermal decomposition at different heating rates. (c) DTG curves of the NADA-DS thermal decomposition at different heating rates.

propagator, while negative values suggest the absence of these tendencies. According to the Yoshida correlation, NADA-DS has an IS value of -0.53 and an EP value of -0.61; the Pfizer correlation gives an IS value of -0.27 and an EP value of -0.53. These results indicate that NADA-DS is not prone to impact sensitivity or explosive propagation.

$$\text{IS (Yoshida)} = \lg(\Delta H_d) - 0.72\lg(T_{\text{onset}} - 25) - 0.98 \quad (2)$$

$$\text{EP (Yoshida)} = \lg(\Delta H_d) - 0.38\lg(T_{\text{onset}} - 25) - 1.67 \quad (3)$$

$$\text{IS (Pfizer)} = \lg(0.75\Delta H_d) - 0.54\lg(T_{\text{init}} - 25) - 0.98 \quad (4)$$

$$\text{EP (Pfizer)} = \lg(0.75\Delta H_d) - 0.285\lg(T_{\text{init}} - 25) - 1.67 \quad (5)$$

where  $\Delta H_d$  is the enthalpy of decomposition (cal/g), and  $T_{\text{onset}}$  and  $T_{\text{init}}$  (°C) are extrapolated onset temperature and initial temperatures.

**3.4.3. Activation Energy of NADA-DS Decomposition.** Activation energy reflects the difficulty of thermal decomposition of a substance, and it is crucial for evaluating potential thermal hazards. It is also a key parameter for the subsequent calculation of TMR<sub>ad</sub>. Therefore, this study employs model-free methods to calculate thermal analysis kinetics based on TGA data.<sup>50</sup> Common methods include the Flynn-Wall-Ozawa (FWO) and the Kissinger-Akahira-Sunose (KAS) methods, with their respective calculation formulas presented in Equations 6 and (7).<sup>51</sup>

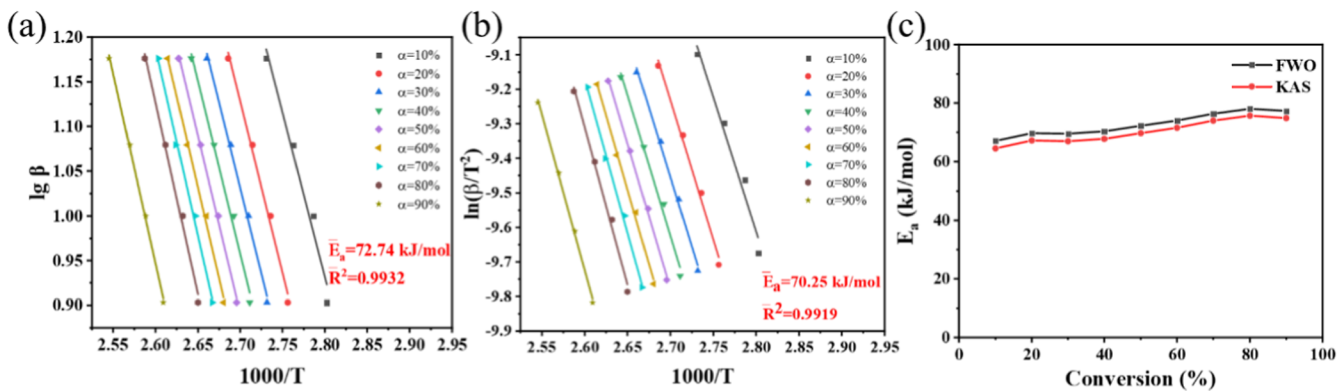


**Figure 9.** Model-free methods to calculate activation energy. (a) Activation energy fitting curves obtained using the FWO method at different conversion rates. (b) Activation energy fitting curves obtained using the KAS method at different conversion rates. (c) Relationship between activation energy and conversion rate.

$$\lg \beta = \lg \frac{AE_a}{RG(a)} - 2.315 - 0.4567 \frac{E_a}{RT} \quad (6)$$

$$\ln \frac{\beta}{T^2} = \ln \left[ \frac{AR}{E_a G(\alpha)} \right] - \frac{E_a}{RT} \quad (7)$$

where  $\beta$  represents the heating rate ( $^{\circ}\text{C}/\text{min}$ ),  $E_a$  denotes the activation energy (kJ/mol),  $R$  signifies the molar gas constant (J/(mol·K)), and  $T$  indicates the temperature (K) corresponding to the same conversion rate at different heating rates.

Figure 9a illustrates the linear fit of  $\lg \beta$  versus  $1000/T$  using the FWO method. According to the slope of each line,  $E_a$  at different conversion rates ( $\alpha$ ) can be determined. The average apparent activation energy ( $\bar{E}_a$ ) is 72.74 kJ/mol, and the average determination coefficient ( $\bar{R}^2$ ) is 0.9932. On the other hand, the KAS method was used to calculate  $E_a$  by fitting  $\ln \frac{\beta}{T^2}$  and  $1000/T$ , and the linear fit is shown in Figure 9b. ( $\bar{E}_a$ ) is 70.25 kJ/mol, and  $\bar{R}^2$  is 0.9919. The activation energies obtained from both methods are closely aligned. Therefore,  $E_a$  of NADA-DS, calculated as the average of the FWO and KAS methods, is 71.50 kJ/mol. As the conversion rate increases,  $E_a$  changes minimally, indicating that NADA-DS decomposition follows a single kinetic mechanism (Figure 9c).

**3.5. Safety Assessment of the Continuous Diazotization Process for NADA.** **3.5.1. Severity of Uncontrolled NADA Diazotization.** EasyMax 402 HFCal reaction calorimeter is widely used in chemical process safety assessments and for measuring the actual heat released during chemical reactions.<sup>52,53</sup> The exothermic nature of the NADA diazotization process was determined using this instrument (Figure 10). During the reaction, a significant amount of heat is rapidly released, causing the reaction temperature ( $T_r$ ) to rise quickly. To mitigate the temperature increase, the reaction calorimeter lowers the jacket temperature ( $T_j$ ) to dissipate the heat. The heat flow curve ( $q_r$ ) approaches zero at around 50 s, indicating that the NADA diazotization reaction is rapid and exothermic, with a maximum heat release rate of 345 W. By integrating the heat flow curve, the reaction enthalpy was determined to be 96.66 kJ/mol.

The severity of a runaway reaction is measured by the adiabatic temperature rise ( $\Delta T_{ad}$ ) during the diazotization reaction. According to eq 8,<sup>54</sup>  $\Delta T_{ad}$  for the NADA diazotization reaction is 11.17 K. When  $\Delta T_{ad} \leq 50$  K, the

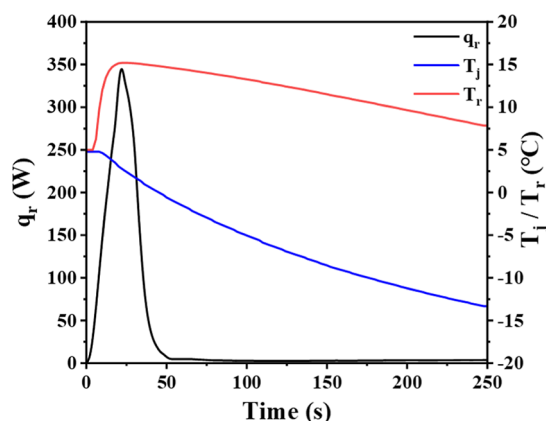


**Figure 10.** Exothermic curve of the NADA diazotization.

hazard level is classified as level 1, suggesting that thermal runaway would have relatively low severity.

$$\Delta T_{ad} = \frac{Q_r}{C_p m} \quad (8)$$

where  $Q_r$  is the total heat release of the diazotization reaction (J);  $C_p$  is the specific heat capacity of the reaction system (J/(g·K)); and  $m$  is the total mass of the reaction system (g).

In the case of cooling failure, the maximum temperature of the diazotization reaction (known as MTSR), is a critical parameter for the safety assessment of diazotization. MTSR is calculated using eq 9,<sup>55</sup> and the results are presented in Table 3.

$$\text{MTSR} = T_p + X_{ac} \times \Delta T_{ad} \quad (9)$$

where  $T_p$  represents the process temperature, set to 20 °C after the process optimization;  $X_{ac}$  denotes the material accumulation level, with a worst-case scenario set to 100%.

**3.5.2. Probability of Uncontrolled NADA Diazotization.** The  $\text{TMR}_{ad}$  was used to assess the probability of worst-case scenarios in uncontrolled reactions, defined as the time required for the reaction to reach its maximum rate under adiabatic conditions. The primary side reaction caused by thermal runaway during the diazotization reaction is NADA-DS thermal decomposition. For a more conservative approach, a zero-order reaction assumption was made, and eq 10<sup>55,56</sup> was used to calculate  $\text{TMR}_{ad}$ . The calculation requires DSC data and the decomposition activation energy. The heat release rate

( $q$ ) at various temperatures can be obtained using eq 11. Figure 11 shows that the  $TMR_{ad}$  is 24 h when the process

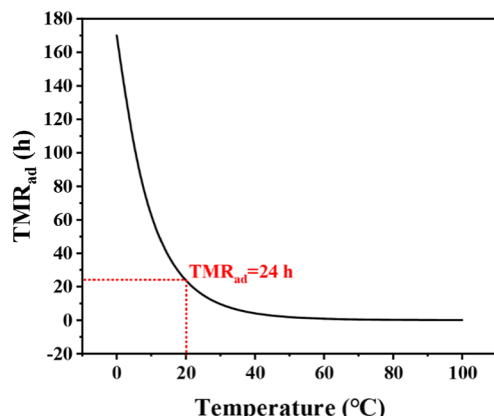


Figure 11. Relationship between diazotization temperature and  $TMR_{ad}$ .

temperature is 20 °C, and the probability of an uncontrolled reaction is classified as level 1, suggesting that such occurrences are rare.

$$TMR_{ad} = \frac{C_p R T^2}{E_a q} \quad (10)$$

where  $C_p$  is the specific heat capacity of the substance (2 J/(g·K)).  $E_a$  is the average activation energy for the decomposition of NADA-DS (71,500 J/mol).  $R$  is the molar gas constant (J/(mol·K)).  $T$  is the initial temperature of the substance (K).  $q$  is the mass-normalized exothermic rate at the investigated temperature (W/g).

$$q = q_{ref} \exp\left(-\frac{E_a}{R}\left(\frac{1}{T} - \frac{1}{T_{ref}}\right)\right) \quad (11)$$

where  $q_{ref}$  is the heat release rate of the substance at near-zero conversion (0.02 W/g).  $T_{ref}$  is the sample temperature at zero conversion (K).

**3.5.3. Assessment of Risk Matrix and Stoessel Criticality Diagram.** To evaluate the thermal hazards of continuous diazotization, a risk matrix combining  $\Delta T_{ad}$  and  $TMR_{ad}$  classifies risk into acceptable, conditionally acceptable, and unacceptable risk.<sup>57</sup> As shown in Table 2, the risk associated with continuous diazotization is classified as an acceptable risk.

Table 2. Thermal Hazard Assessment Using the Risk Matrix for Continuous Diazotization Process

$\Delta T_{ad}$ (K)	severity	$TMR_{ad}$ (h)	possibility	thermal hazard assessment
11.17	1	24	1	acceptable risk

The critical temperatures from the Stoessel criticality diagram<sup>58</sup> are listed in Table 3. MTT, defined as the maximum temperature for technical reasons, is selected based on the

Table 3. Temperatures to Determine the Criticality Class of the Continuous Diazotization Process

$T_p$ (°C)	MTSR (°C)	MTT (°C)	$T_{D0.05}$ (°C)	Class
20	31.17	100	105.75	1

solvent's boiling point due to the open nature of the reaction system.  $T_{D0.05}$  represents the process temperature corresponding to  $TMR_{ad}$  of 0.05 h. With continuous flow, the residence time of the material in the dynamic tubular reactor does not exceed 0.05 h, indicating that uncontrolled reactions are unlikely to reach the maximum reaction rate at lower temperatures and shorter residence times. Therefore,  $T_{D0.05}$  is used instead of TD24 as the critical parameter for the safety assessment of the continuous diazotization process. The critical level for the NADA continuous diazotization process is determined to be level 1 based on ( $T_p < MTSR < MTT < T_{D0.05}$ ), indicating low risk.

## 4. CONCLUSION

In this study, we conducted a multistep continuous heterogeneous synthesis of C.I. Reactive Red 195 using a dynamic tubular reactor for the first time, achieving a throughput of 120 L/h and a yield of 736 kg/day. Compared to the commercial dye, the purity of the synthetic dye increased by 20%, and its K/S value rose from 19.07 to 22.16, significantly enhancing dyeing performance.

NCI and EDA analyses reveal that NADA-DS molecule aggregation is primarily driven by dispersion forces. Furthermore, AIMD simulation results show that once aggregates form, they exhibit high stability, making the dissociation process relatively difficult. This reduces the contact area between NADA-DS molecules and water, leading to precipitation from the aqueous solution.

The initial decomposition temperature of NADA-DS is 71.89 °C, with a decomposition enthalpy of 227.95 J/g and a thermal weight loss rate of approximately 15%. Calculations based on Yoshida and Pfizer's mathematical correlations suggest that NADA-DS has no potential for impact sensitivity or explosion propagation. The average activation energy for the decomposition of NADA-DS is 71.50 kJ/mol. Additionally, the possibility and severity of thermal runaway during continuous diazotization of NADA are both low. The risk matrix evaluation shows the acceptable risk of continuous diazotization, and the Stoessel criticality diagram classifies it as level 1, indicating a lower process hazard.

In summary, this work offers a useful reference for the industrial transition of water-soluble azo dyes from batch to continuous production.

## ■ ASSOCIATED CONTENT

### Supporting Information

The Supporting Information is available free of charge at <https://pubs.acs.org/doi/10.1021/acs.oprd.Sc00055>.

Characterization of mixing; continuous flow experimental setup (PDF)

## ■ AUTHOR INFORMATION

### Corresponding Author

Shufen Zhang — State Key Laboratory of Fine Chemicals, Frontier Science Center for Smart Materials, Dalian University of Technology, Dalian 116024, China;  
<sup>✉</sup> [orcid.org/0000-0003-3390-4199](https://orcid.org/0000-0003-3390-4199); Email: [zhangshf@dlut.edu.cn](mailto:zhangshf@dlut.edu.cn)

**Authors**

- Lei Li — State Key Laboratory of Fine Chemicals, Frontier Science Center for Smart Materials, Dalian University of Technology, Dalian 116024, China
- Xinyu Ye — State Key Laboratory of Fine Chemicals, Frontier Science Center for Smart Materials, Dalian University of Technology, Dalian 116024, China
- Huaixi Liu — State Key Laboratory of Fine Chemicals, Frontier Science Center for Smart Materials, Dalian University of Technology, Dalian 116024, China
- Rongwen Lu — State Key Laboratory of Fine Chemicals, Frontier Science Center for Smart Materials, Dalian University of Technology, Dalian 116024, China;  
✉ orcid.org/0000-0002-2210-3380
- Bingtao Tang — State Key Laboratory of Fine Chemicals, Frontier Science Center for Smart Materials, Dalian University of Technology, Dalian 116024, China;  
✉ orcid.org/0000-0001-5201-9924

Complete contact information is available at:  
<https://pubs.acs.org/10.1021/acs.oprd.5c00055>

**Notes**

The authors declare no competing financial interest.

**ACKNOWLEDGMENTS**

This work was financially supported by the National Natural Science Foundation of China (22238002), the National Key R&D Program of China (2017YFB0307401), the Research and Innovation Team Project of Dalian University of Technology (DUT2022TB10), and the Fundamental Research Funds for the Central Universities (DUT22LAB610).

**REFERENCES**

- (1) Belowar, S.; Rahamatolla, M.; Islam, S.; Jalil, M. A.; Hossain, S.; Saeed, M. A.; Rahman Bhuiyan, M. M.; Kazi, F.; Shekh, S. Design, synthesis, and characterization of a novel pH-responsive azo dye incorporating a 1,3,4-thiadiazole ring for advanced textile applications. *Dyes Pigm.* **2024**, *231*, 112410.
- (2) Nitu, S.; Milea, M. S.; Boran, S.; Mosoarca, G.; Zamfir, A. D.; Popa, S.; Funar-Timofei, S. Experimental and Computational Study of Novel Pyrazole Azo Dyes as Colored Materials for Light Color Paints. *Materials* **2022**, *15* (16), 5507.
- (3) Al-Degs, Y. S. Determination of three dyes in commercial soft drinks using HLA/GO and liquid chromatography. *Food Chem.* **2009**, *117* (3), 485–490.
- (4) Haroun, A. A.; Mansour, H. F. New approaches for the reactive dyeing of the retanned carbohydrate crust leather. *Dyes Pigm.* **2008**, *76* (1), 213–219.
- (5) Feng, G.; Zhu, M.; Liu, L.; Li, C. A quantitative one-pot synthesis method for industrial azo pigments with recyclable wastewater. *Green Chem.* **2019**, *21* (7), 1769–1776.
- (6) Guerra, E.; Llompart, M.; Garcia-Jares, C. Analysis of Dyes in Cosmetics: Challenges and Recent Developments. *Cosmetics* **2018**, *5* (3), 47.
- (7) Sharma, P.; Rane, N.; Gurram, V. K. Synthesis and QSAR studies of pyrimido[4,5-d]pyrimidine-2,5-dione derivatives as potential antimicrobial agents. *Bioorg. Med. Chem. Lett.* **2004**, *14* (16), 4185–4190.
- (8) Benkhaya, S.; M'Rabet, S.; El Harfi, A. Classifications, properties, recent synthesis and applications of azo dyes. *Heliyon* **2020**, *6* (1), No. e03271.
- (9) Ranade, V. V.; Sharma, M. K.; Kulkarni, A. A. CRE for MAGIC (modular, agile, intensified & continuous) processes. *Chem. Eng. J.* **2015**, *278*, 454–468.
- (10) Firth, J. D.; Fairlamb, I. J. S. A Need for Caution in the Preparation and Application of Synthetically Versatile Aryl Diazonium Tetrafluoroborate Salts. *Org. Lett.* **2020**, *22* (18), 7057–7059.
- (11) Partington, S.; Waldrum, S. P. Runaway Reaction During Production of an Azo Dye Intermediate. *Process Saf. Environ. Prot.* **2002**, *80* (1), 33–39.
- (12) Shukla, C. A.; Kute, M. S.; Kulkarni, A. A. Towards sustainable continuous production of azo dyes: possibilities and techno-economic analysis. *Green Chem.* **2021**, *23* (17), 6614–6624.
- (13) Ullrich, R.; Grewer, T. Decomposition of aromatic diazonium compounds. *Thermochim. Acta* **1993**, *225* (2), 201–211.
- (14) Sheng, M.; Frurip, D.; Gorman, D. Reactive chemical hazards of diazonium salts. *J. Loss Prev. Process Ind.* **2015**, *38*, 114–118.
- (15) Nielsen, M. A.; Nielsen, M. K.; Pittelkow, T. Scale-Up and Safety Evaluation of a Sandmeyer Reaction. *Org. Process Res. Dev.* **2004**, *8* (6), 1059–1064.
- (16) Zhang, Q.; Guo, Y. L.; Jin, M. P. Thermal hazard classification of the diazotization reaction of glycine methyl ester. *Safety Health & Environment (China)* **2019**, *19* (06), 31–36.
- (17) Cheng, L.; Liu, Y.; Sun, J.; Xu, Y. Z. Thermal hazard assessment for diazotization of 2-methoxy-4-nitroaniline. *Chem. Eng.* **2022**, *50* (12), 61–65 + 71.
- (18) Xie, C.; Yuan, Y.; Wang, B.; Du, L. Research on the decomposition kinetics and thermal hazards of aniline diazonium salt. *Thermochim. Acta* **2022**, *709*, 179156.
- (19) Souza, E. L. S. d.; Chorro, T. H. D.; Correia, C. R. D. Thermal analysis of arenediazonium tetrafluoroborate salts: Stability and hazardous evaluation. *Process Saf. Environ. Prot.* **2023**, *177*, 69–81.
- (20) Schotten, C.; Leprevost, S. K.; Yong, L. M.; Hughes, C. E.; Harris, K. D. M.; Browne, D. L. Comparison of the Thermal Stabilities of Diazonium Salts and Their Corresponding Triazenes. *Org. Process Res. Dev.* **2020**, *24* (10), 2336–2341.
- (21) Bondarev, A. A.; Naumov, E. V.; Kassanova, A. Z.; Krasnokutskaya, E. A.; Stankevich, K. S.; Filimonov, V. D. First Study of the Thermal and Storage Stability of Arenediazonium Triflates Comparing to 4-Nitrobenzenediazonium Tosylate and Tetrafluoroborate by Calorimetric Methods. *Org. Process Res. Dev.* **2019**, *23* (11), 2405–2415.
- (22) Xue, H.; Qi, T.; Su, W.; Wu, K.-J.; Su, A. Heterogeneous Continuous Flow Hydrogenation of Hexafluoroacetone Trihydrate and Its Kinetic Modeling. *Ind. Eng. Chem. Res.* **2023**, *62* (15), 6121–6129.
- (23) Al Azri, N.; Patel, R.; Ozbuyukkaya, G.; Kowall, C.; Cormack, G.; Proust, N.; Enick, R.; Veser, G. Batch-to-Continuous transition in the specialty chemicals Industry: Impact of operational differences on the production of dispersants. *Chem. Eng. J.* **2022**, *445*, 136775.
- (24) Chen, J.; Xie, X.; Liu, J.; Yu, Z.; Su, W. Revisiting aromatic diazotization and aryl diazonium salts in continuous flow: highlighted research during 2001–2021. *React. Chem. Eng.* **2022**, *7* (6), 1247–1275.
- (25) Shi, Z.; Wang, X.; Yin, D.; Li, W.; Liu, D.; Zhou, X. High-Flux Continuous-Flow Synthesis of C.I. Pigment Yellow 12 from Clear Alkaline Solutions of the Coupling Component. *Org. Process Res. Dev.* **2022**, *26* (3), 661–669.
- (26) Pennemann, H.; Forster, S.; Kinkel, J.; Hessel, V.; Löwe, H.; Wu, L. Improvement of Dye Properties of the Azo Pigment Yellow 12 Using a Micromixer-Based Process. *Org. Process Res. Dev.* **2005**, *9* (2), 188–192.
- (27) Wang, F. J.; Huang, J. P.; Xu, J. H. Continuous-Flow Synthesis of the Azo Pigment Yellow 14 Using a Three-Stream Micromixing Process. *Org. Process Res. Dev.* **2019**, *23* (12), 2637–2646.
- (28) Gao, J. R.; Li, A. K.; Xu, M.; Ye, Q. The method for preparing CI REACTIVE Red 195s is continuously coupled in a kind of microchannel. CN 107325059 A, 2017.
- (29) Wang, F. J.; Ding, Y. C.; Xu, J. H. Continuous-Flow Synthesis of Pigment Red 146 in a Microreactor System. *Ind. Eng. Chem. Res.* **2019**, *58* (36), 16338–16347.
- (30) Sharma, B. M.; Atapalkar, R. S.; Kulkarni, A. A. Continuous flow solvent free organic synthesis involving solids (reactants/

- products) using a screw reactor. *Green Chem.* **2019**, *21* (20), 5639–5646.
- (31) Bourne, J. R.; Kut, O. M.; Lenzner, J.; Maire, H. Kinetics of the diazo coupling between 1-naphthol and diazotized sulfanilic acid. *Ind. Eng. Chem. Res.* **1990**, *29* (9), 1761–1765.
- (32) Zhang, H.; Kopfmüller, T.; Achermann, R.; Zhang, J.; Teixeira, A.; Shen, Y.; Jensen, K. F. Accessing multidimensional mixing via 3D printing and showerhead micromixer design. *AIChE J.* **2020**, *66* (4), No. e16873.
- (33) Bourne, J. R.; Maire, H. Micromixing and fast chemical reactions in static mixers. *Chem. Eng. Process.* **1991**, *30* (1), 23–30.
- (34) Liang, D.; Zhang, S. A Contraction-expansion Helical Mixer in the Laminar Regime. *Chin. J. Chem. Eng.* **2014**, *22* (3), 261–266.
- (35) Smallwood, C. J.; McAllister, M. A. Characterization of Low-Barrier Hydrogen Bonds. 7. Relationship between Strength and Geometry of Short-Strong Hydrogen Bonds. The Formic Acid–Formate Anion Model System. An ab Initio and DFT Investigation. *J. Am. Chem. Soc.* **1997**, *119* (46), 11277–11281.
- (36) Grimme, S.; Ehrlich, S.; Goerigk, L. Effect of the damping function in dispersion corrected density functional theory. *J. Comput. Chem.* **2011**, *32* (7), 1456–1465.
- (37) Grimme, S.; Antony, J.; Ehrlich, S.; Krieg, H. A consistent and accurate ab initio parametrization of density functional dispersion correction (DFT-D) for the 94 elements H–Pu. *J. Chem. Phys.* **2010**, *132* (15), 154104.
- (38) Cossi, M.; Barone, V.; Cammi, R.; Tomasi, J. Ab initio study of solvated molecules: A new implementation of the polarizable continuum model. *Chem. Phys. Lett.* **1996**, *255*, 327–335.
- (39) Lu, T.; Chen, F. Multiwfn: A multifunctional wavefunction analyzer. *J. Comput. Chem.* **2012**, *33* (5), 580–592.
- (40) Humphrey, W.; Dalke, A.; Schulten, K. VMD: Visual molecular dynamics. *J. Mol. Graphics* **1996**, *14* (1), 33–38.
- (41) Parrish, R. M.; Burns, L. A.; Smith, D. G. A.; Simmonett, A. C.; DePrince, A. E., III; Hohenstein, E. G.; Bozkaya, U.; Sokolov, A. Y.; Di Remigio, R.; Richard, R. M.; et al. Psi4 1.1: An Open-Source Electronic Structure Program Emphasizing Automation, Advanced Libraries, and Interoperability. *J. Chem. Theory Comput.* **2017**, *13* (7), 3185–3197.
- (42) Grimme, S.; Bannwarth, C.; Shushkov, P. A Robust and Accurate Tight-Binding Quantum Chemical Method for Structures, Vibrational Frequencies, and Noncovalent Interactions of Large Molecular Systems Parametrized for All spd-Block Elements ( $Z = 1$ –86). *J. Chem. Theory Comput.* **2017**, *13* (5), 1989–2009.
- (43) Shukla, C. A.; Kulkarni, A. A.; Ranade, V. V. Selectivity engineering of the diazotization reaction in a continuous flow reactor. *React. Chem. Eng.* **2016**, *1* (4), 387–396.
- (44) Zheng, P.; Luo, Z.-H.; Wei, H.-L. Kinetic Measurement and Modeling of a Slow-Rate Diazo Coupling Reaction. *Ind. Eng. Chem. Res.* **2023**, *62* (29), 11585–11594.
- (45) Wang, N.; Zhou, J.; Zhang, Y.; Ge, Y.; Li, N. Continuous Flow Synthesis of Ethyl Diazoacetate and CFD Analysis of Micromixing Efficiency in a Microreactor. *Ind. Eng. Chem. Res.* **2024**, *63* (32), 14002–14017.
- (46) Pipitone, G.; Hensley, A. J. R.; Omoniyi, A.; Zoppi, G.; Pirone, R.; Bensaid, S. Unravelling competitive adsorption phenomena in the aqueous phase reforming of carboxylic acids on Pt catalysts: An experimental and theoretical study. *Chem. Eng. J.* **2024**, *482*, 148902.
- (47) Bjelić, A.; Likozar, B.; Grilc, M. Scaling of lignin monomer hydrogenation, hydrodeoxygenation and hydrocracking reaction micro-kinetics over solid metal/acid catalysts to aromatic oligomers. *Chem. Eng. J.* **2020**, *399*, 125712.
- (48) Horvath-Gerber, F.; Ohlig, D.; Hii, K. K. M.; Deadman, B.; Attrill, R. P.; Hellgardt, K. Liquizald—Thermally Stable N-Nitrosamine Precursor for Diazomethane. *Org. Process Res. Dev.* **2024**, *28* (2), 597–608.
- (49) Green, S. P.; Wheelhouse, K. M.; Payne, A. D.; Hallett, J. P.; Miller, P. W.; Bull, J. A. Thermal Stability and Explosive Hazard Assessment of Diazo Compounds and Diazo Transfer Reagents. *Org. Process Res. Dev.* **2020**, *24* (1), 67–84.
- (50) Chen, Z.; Wang, Y.; Ji, W.; Guo, X.; Liu, X.; Ma, C.; Guo, J.; Su, Y. Thermal Decomposition Kinetics of Benzoyl Peroxide Based on Thermogravimetric Analysis and DFT Simulations. *Org. Process Res. Dev.* **2024**, *28* (9), 3674–3684.
- (51) Li, Z.-P.; Huang, A.-C.; Tang, Y.; Zhou, H.-L.; Liu, Y.-C.; Huang, C.-F.; Shu, C.-M.; Xing, Z.-X.; Jiang, J.-C. Thermokinetic prediction and safety evaluation for toluene sulfonation process and product using calorimetric technology. *J. Therm. Anal. Calorim.* **2022**, *147* (21), 12177–12186.
- (52) Yang, Q.; Sheng, M.; Huang, Y. Potential Safety Hazards Associated with Using N,N-Dimethylformamide in Chemical Reactions. *Org. Process Res. Dev.* **2020**, *24* (9), 1586–1601.
- (53) Wang, Z.; Cao, D.; Xu, Z.; Wang, J.; Chen, L. Thermal safety study on the synthesis of HMX by nitrourea method. *Process Saf. Environ. Prot.* **2020**, *137*, 282–288.
- (54) Sun, Y.; Ni, L.; Papadaki, M.; Zhu, W.; Jiang, J.; Mashuga, C.; Wilhite, B.; Mannan, M. S. Process hazard evaluation for catalytic oxidation of 2-octanol with hydrogen peroxide using calorimetry techniques. *Chem. Eng. J.* **2019**, *378*, 122018.
- (55) Keller, A.; Stark, D.; Fierz, H.; Heinzle, E.; Hungerbühler, K. Estimation of the time to maximum rate using dynamic DSC experiments. *J. Loss Prev. Process Ind.* **1997**, *10* (1), 31–41.
- (56) Leveneur, S. Thermal Safety Assessment through the Concept of Structure–Reactivity: Application to Vegetable Oil Valorization. *Org. Process Res. Dev.* **2017**, *21* (4), 543–550.
- (57) Jiang, W.; Ni, L.; Jiang, J.; Chen, Q.; Chen, Z.; Ye, S. Thermal hazard and reaction mechanism of the preparation of adipic acid through the oxidation with hydrogen peroxide. *AIChE J.* **2021**, *67* (1), No. e17089.
- (58) Stoessel, F. Planning protection measures against runaway reactions using criticality classes. *Process Saf. Environ. Prot.* **2009**, *87* (2), 105–112.

**CAS INSIGHTS™****EXPLORE THE INNOVATIONS SHAPING TOMORROW**

Discover the latest scientific research and trends with CAS Insights. Subscribe for email updates on new articles, reports, and webinars at the intersection of science and innovation.

**Subscribe today**